

Massive disc galaxies in cosmological hydrodynamical simulations are too dark matter-dominated

A. Marasco¹, L. Posti², K. Oman³, B. Famaey², G. Cresci¹ and F. Fraternali⁴

¹ INAF - Osservatorio Astrofisico di Arcetri, Largo E. Fermi 5, 50127, Firenze, Italy
e-mail: antonino.marasco@inaf.it

² Université de Strasbourg, CNRS UMR 7550, Observatoire astronomique de Strasbourg, 11 rue de l'Université, 67000 Strasbourg, France

³ Institute for Computational Cosmology, Department of Physics, Durham University, South Road, Durham DH1 3LE, UK

⁴ Kapteyn Astronomical Institute, University of Groningen, Postbus 800, 9700 AV Groningen, The Netherlands

Received ; accepted

ABSTRACT

We investigate the disc-halo connection in massive ($M_\star > 5 \times 10^{10} M_\odot$) disc galaxies from the cosmological hydrodynamical simulations EAGLE and IllustrisTNG, and compare it with that inferred from the study of H I rotation curves in nearby massive spirals from the Spitzer Photometry and Accurate Rotation Curves (SPARC) dataset. We find that discrepancies between the simulated and observed discs arise both on global and on local scales. Globally, the simulated discs inhabit halos that are a factor ~ 4 (in EAGLE) and ~ 2 (in IllustrisTNG) more massive than those derived from the rotation curve analysis of the observed dataset. We also use synthetic rotation curves of the simulated discs to demonstrate that the recovery of the halo masses from rotation curves are not systematically biased. We find that the simulations predict dark-matter dominated systems with stellar-to-total enclosed mass ratios that are a factor of 1.5–2 smaller than real galaxies at all radii. This is an alternative manifestation of the ‘failed feedback problem’, since it indicates that simulated halos hosting massive discs have been too inefficient at converting their baryons into stars, possibly due to an overly efficient stellar and/or AGN feedback implementation.

Key words. galaxies: kinematics and dynamics – galaxies: halos – galaxies: spiral – Methods: numerical

1. Introduction

In the standard Λ cold dark matter (Λ CDM) framework, galaxies form via the cooling and gravitational collapse of baryonic matter within the potential wells provided by the dark matter halos (e.g. White & Rees 1978). Assuming a universal baryonic-to-dark matter fraction, $f_b \equiv \Omega_b/\Omega_c \simeq 0.188$ (Planck Collaboration et al. 2018) one should expect that, on average, halos of mass M_{halo} host gas reservoirs with masses of $f_b M_{\text{halo}}$ out of which galaxies can form. However, the efficiency of the baryons-to-stars conversion process, $f_\star = M_\star/(f_b M_{\text{halo}})$, along with the morphological, kinematic and chemical properties of the resulting system, depends on the complex interplay between the various physical processes that orchestrate galaxy evolution, and cannot easily be predicted a priori. Independent estimates of the so-called galaxy-halo connection at different masses, different epochs and for galaxies of different morphological types are required to provide constraints on the whole theoretical framework of galaxy formation.

One of the key ingredients of the galaxy-halo connection is the relation between M_\star and M_{halo} (or, equivalently, between M_\star and f_\star), the stellar-to-halo mass relation (SHMR, see Wechsler & Tinker 2018, for a recent review). This relation is commonly probed via a semi-empirical technique known as abundance matching (AM), which relates central galaxies to halos by matching the observed galaxy stellar mass function to the theoretical halo mass function, under the assumption that stellar mass increases monotonically with the mass of the host halo (Vale & Ostriker 2004; Behroozi et al. 2010; Moster et al. 2013;

Kravtsov et al. 2018). Taken together, different AM studies build up a coherent picture where f_\star peaks at $\sim 20\%$ in L_\star galaxies, and rapidly decreases at lower and higher masses. Such global inefficiency of baryon-to-star conversion is interpreted as evidence for ‘negative’ feedback from star formation itself (for $M_{\text{halo}} \lesssim 10^{12} M_\odot$) and Active Galactic Nuclei (AGN) activity (for $M_{\text{halo}} \gtrsim 10^{12} M_\odot$).

Observationally, the SHMR can be probed via different techniques such as galaxy-galaxy weak lensing (Mandelbaum et al. 2006; Leauthaud et al. 2012), satellite kinematics (van den Bosch et al. 2004; More et al. 2011; van den Bosch et al. 2019), internal galaxy dynamics (Persic et al. 1996; Cappellari et al. 2013; Read et al. 2017) or a combination of these (Dutton et al. 2010). While generally confirming the scenario predicted by AM techniques, some of these studies have signalled a bimodality in the SHMR for the most luminous late- and early-type systems, with the former systematically occupying halos with $M_{\text{halo}} < 10^{13} M_\odot$, and the latter being preferentially located in groups and clusters with $M_{\text{halo}} > 10^{13} M_\odot$. However, the paucity of spirals at $M_\star > 10^{11} M_\odot$ makes precise measurements challenging, and it is unclear whether the observed bimodality arises naturally from the shape and scatter of the SHMR (Moster et al. 2019) or is symptomatic of different star formation efficiencies associated to different galaxy types (Mandelbaum et al. 2016).

Recently, Posti et al. (2019a, hereafter PFM19) have determined the SHMR in a sample of nearby isolated disc galaxies from the Spitzer Photometry and Accurate Rotation Curves (SPARC, Lelli et al. 2016) dataset via the mass decomposition of their H I rotation curves. Their results show the existence of

a monotonic SHMR for discs spanning more than four orders of magnitude in M_\star , with the most massive spirals inhabiting ‘light’ dark matter halos and having f_\star close to unity, in striking contrast with predictions from AM methods. The existence of such a monotonic SHMR is intimately connected to the monotonicity of the relations between the stellar masses, sizes and rotational velocities of discs (Posti et al. 2019b), and is evidence for the presence of different pathways for the formation of early- and late-type galaxies. This result is not *per se* incompatible with AM, assuming that the high-mass end of the galaxy stellar mass function is dominated by early-type systems, but outlines the existence of a class of galaxies for which feedback has failed at quenching the star formation efficiency (the ‘failed feedback problem’, Posti et al. 2019b). Nonetheless, while this discrepancy was noted on global scales, the main culprit, i.e. feedback, acts on the scales of galactic discs. This leads us to ask whether the detailed structure of discs is also affected by this phenomenon; in other words, whether the local dynamical structure of real massive spirals behaves as expected from current state-of-the-art models.

In this work we compare these observational results with the predictions from two state-of-the-art cosmological hydrodynamical simulation suites, EAGLE (Schaye et al. 2015) and IllustrisTNG (Pillepich et al. 2018). While the parameters of these simulations are tuned to reproduce a number of observables at $z = 0$, including the galaxy stellar mass function, the detailed connection between galaxies and their hosting halos is not forced ‘by hand’ but follows from the complex physics of galaxy formation, which is treated self-consistently. These models are adequate to resolve the morphology and internal dynamics for several tens of massive spirals at $z = 0$, which makes them the best possible tools to investigate the connection between galaxy type and the SHMR.

2. Simulated and observed galaxy samples

We focus our analysis on isolated, regularly-rotating disc galaxies with stellar masses M_\star larger than $5 \times 10^{10} M_\odot$. As shown by PFM19, in this mass range the derived f_\star of discs diverges significantly from the behaviour predicted by AM methods. Our observed sample consists therefore of the 21 massive discs selected by PFM19 in this mass range. We note that the original SPARC sample includes additional 11 massive galaxies which have been excluded in the study of PFM19, either because of their low inclination (2) or because the rotation curve modelling led to a poor inference on M_\star or M_{halo} (9). The latter case comprises also 3 edge-on spirals for which the rotation curve in the inner regions suffers from projection effects.

We build our simulated galaxy sample using two suites of very well-known, publicly available cosmological hydrodynamical simulations of galaxy formation in the Λ CDM framework: EAGLE and IllustrisTNG. Both simulation suites follow self-consistently the formation and evolution of galaxies and of their environments, and include treatments for star formation, stellar evolution, black-hole accretion, feedback from supernovae and AGN, primordial and metal-line gas cooling and, in the case of IllustrisTNG, the amplification and evolution of seed magnetic fields. The parameters of both models are calibrated to output a ‘realistic’ population of galaxies at $z = 0$ in terms of their number densities, sizes, central black-hole masses and star formation rates. Differences between the predictions of the two models are most often caused by: differences in the treatment of the ‘sub-grid’ physics (e.g. stellar and AGN feedback implementation); differences in the accuracy with which the model calibration suc-

ceeds in reproducing the observed calibrators; the inclusion of magnetic field physics in IllustrisTNG (absent in EAGLE); and the use of different solvers for the (magneto-)hydrodynamical equations¹. Further details on these simulations can be found in Schaye et al. (2015); Crain et al. (2015) and Pillepich et al. (2018).

The runs which we consider here are Ref-L0100N1504 (in EAGLE) and TNG100-1 (in IllustrisTNG). The former (latter) considers a cubic volume with side length of 100 Mpc (111 Mpc) and uses dark matter particles with a mass of $9.7 (7.4) \times 10^6 M_\odot$, gas particles (cells) with initial masses $1.8 (1.4) \times 10^6 M_\odot$, and a gravitational softening length of 0.70 (0.74) kpc. Thus, both runs are adequate to resolve the morphology and the kinematics of hundreds of galaxies in the mass range of interest.

Using the EAGLE and IllustrisTNG galaxy catalogues from the public releases of McAlpine et al. (2016) and Nelson et al. (2019), we select all central galaxies at $z = 0$ in our stellar mass range of interest². In order to extract a subsample of regularly rotating disc galaxies, we use two morpho-kinematical estimators: the ratio between stellar rotational velocity and velocity dispersion (\mathcal{R}_\star), and the stellar disc fraction (\mathcal{F}_\star). The former is given by the ratio between the mass-weighted median rotational speed for stars orbiting within the galactic plane and their velocity dispersion perpendicular to it, while the latter is based on the fraction of non-counter-rotating stars within $R < 30$ kpc (Thob et al. 2019). While both estimators were already available in the EAGLE catalogues, only \mathcal{F}_\star was pre-computed for IllustrisTNG, so we determined \mathcal{R}_\star for our subsample using the procedure of Thob et al. (2019).

We label as ‘discs’ those systems having $\mathcal{R}_\star > 1.7$ and $\mathcal{F}_\star > 0.7$. These thresholds ensure that resulting fraction of disc galaxies decreases as a function of M_\star , following a trend which is compatible with observations from the GAMA survey (Driver et al. 2011) derived by Moffett et al. (2016), as we show in the first panel of Fig. 1. We stress that the comparison is purely qualitative, as the morphological classification used in GAMA is based on visual inspection of optical and near-infrared images. Yet, both EAGLE and IllustrisTNG galaxies seem to be in agreement with the observed trend. As an additional step, we visually inspected the morphology of the simulated discs using the (synthetic) edge-on and face-on composite optical images available from the two simulation databases, and discarded those (few) galaxies which either appeared to be strongly warped or showed visible signs of recent interactions with companions. These selections resulted in a final sample of 46 systems for EAGLE and 130 systems for IllustrisTNG. We stress, and discuss below, that our results do not depend on the adopted thresholds for \mathcal{R}_\star and \mathcal{F}_\star . Tables listing the main properties of the galaxies studied in this work, along with examples of synthetic optical images are presented in Appendix A.

In the central panel of Fig. 1 we compare the stellar Tully-Fisher relation (TFR, Tully & Fisher 1977) for our sample of simulated galaxies and for the SPARC sample. The definition of v_{flat} - the velocity at which the rotation curve flattens - used for the simulated discs is based on their circular velocity profile derived assuming spherical symmetry, $v_c = \sqrt{GM($R)/R}$, which we compute for each galaxy in our sample, along with its decomposition into the separate contributions of stars, gas (in the$

¹ EAGLE uses a modified version of the SPH code GADGET-2 (Springel 2005) while IllustrisTNG uses the moving-mesh code AREPO (Springel 2010).

² In each subhalo, M_\star is computed within a sphere of 30 kpc of radius centred on the minimum of the gravitational potential.

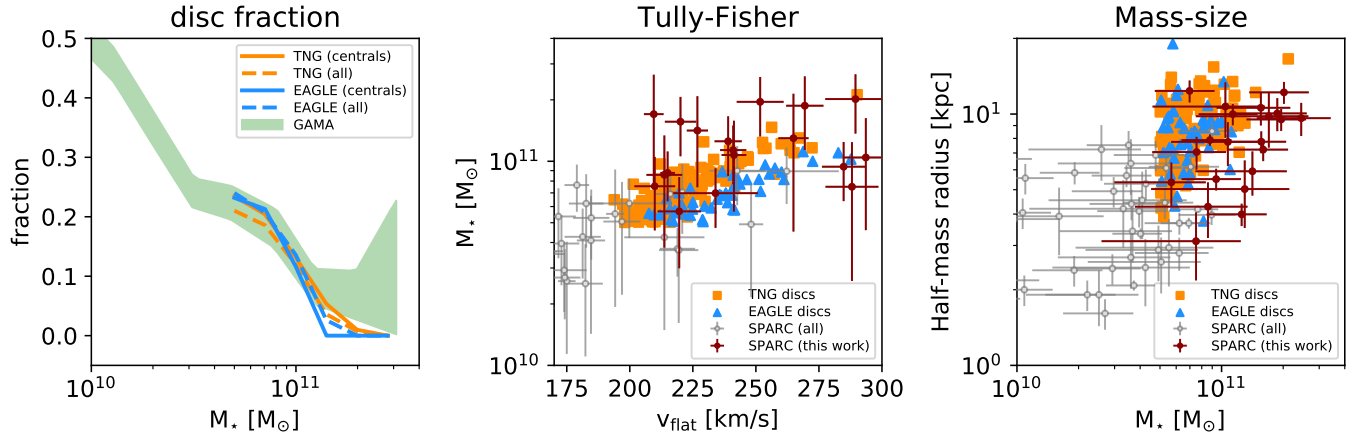


Fig. 1. *Left panel:* fraction of disc galaxies as a function of their stellar mass in EAGLE (blue lines) and IllustrisTNG (orange lines), compared to that measured in the GAMA survey by Moffett et al. (2016, shaded green area). Solid lines show centrals only; dashed lines include also satellites. *Central panel:* stellar Tully-Fisher relation for our subsample of simulated (central) discs with M_* $> 5 \times 10^{10} M_\odot$ in EAGLE (blue triangles) and IllustrisTNG (orange squares), compared with the population of nearby spirals from the SPARC dataset (circles with error bars). Galaxies from SPARC are shown as circles with error-bars. Filled red circles are used for the sub-sample of massive discs studied in this work. *Right panel:* stellar mass-size relation for the same systems.

case of IllustrisTNG, including ‘wind’ particles), and dark matter. To ensure the best possible comparison with the data, we truncate our v_c profiles at the ‘H_I radius’ as determined from the H_I mass-size relation of Lelli et al. (2016)³, under the assumption that the simulated discs have an H_I content analogous to that of SPARC galaxies with similar stellar mass. This stratagem allows us to bypass the various pitfalls that arise when dealing with rotation curves derived directly from ‘simulated’ H_I data (e.g. Oman et al. 2019, see also Section 4), and is based on the ansatz that H_I rotation curves in real galaxies are excellent proxies for v_c . We have verified visually that the vast majority of v_c profiles flatten out in the outer disc regions (see Appendix A) and that rotational speeds extracted in the proximity of R_{HI} are good proxies for v_{flat} . We therefore set v_{flat} to the mean velocity measured in the interval between R_{HI} and 3 kpc inward of this radius.

In general, there is a very good agreement between the simulated and the observed data, with the former producing a very narrow sequence in the $v_{\text{flat}} - M_*$ plane passing in between the SPARC data points. However, important differences appear at $M_* \gtrsim 10^{11} M_\odot$, where most simulated discs have large ($> 250 \text{ km s}^{-1}$) v_{flat} while observed spirals show a wider distribution of rotational speeds, with a mean shifted towards lower velocities. In the right panel of Fig. 1 we compare the size- M_* relation for the SPARC and the simulated galaxies, under the assumption that the 3.6 μm effective radii, used for the observed sample, are good proxies for the half- M_* radii, used for the simulated sample. Also in this case the agreement is good, but less accurate, with the simulated galaxies occupying preferentially the upper tail of the observed size distribution at fixed M_* .

In summary, overall good agreement exists between simulated and real discs in terms of global scaling relations, although the former have slightly larger sizes and rotational speeds than the latter, especially at the high- M_* end. As we show below, these small differences become more evident when investigating the disc-halo connection.

³ We note that discs in EAGLE and IllustrisTNG reproduces well this relation (Bahé et al. 2016; Diemer et al. 2019).

3. Results

3.1. Global disc-halo connection

PFM19 determined the stellar and dark matter content of SPARC galaxies via the analysis of their H_I rotation curves and of their 3.6 μm *Spitzer* photometry. Their Bayesian approach led them to infer unimodal, well defined posteriors on the mass-to-light ratio and on M_{halo} for 137 galaxies. In the simulations, we have the luxury of knowing precisely the stellar and dark matter content of our galaxies, which opens the possibility to two complementary approaches: we can either use the stellar and halo masses reported in the catalogues, or carry out rotation curve decompositions using the same v_c profiles discussed in Section 2. We present the results derived with the former approach below, while in Appendix B we demonstrate that they do not change if we use the latter, more observationally-oriented method. This is a confirmation of the validity and robustness of the methodology of PFM19: mass-decomposition of H_I rotation curves is a powerful tool to determine halo masses in a ΛCDM universe, at least in the mass regime studied here.

In Fig. 2 we show the relation between f_* and M_* for the whole population of massive centrals in EAGLE and IllustrisTNG, for the subsample of simulated discs and for the SPARC sample, along with the prediction from the AM method of Moster et al. (2013). In general, the SPARC massive discs have higher f_* compared to the simulated galaxies, which is expected given that spheroids dominate in the high-mass regime. On average, at fixed M_* , IllustrisTNG centrals have a higher f_* than EAGLE centrals due to an overall higher normalization of the stellar mass function in this mass range, which implies that more numerous (i.e., less massive) halos are populated by galaxies of that M_* . This also explains why we find a greater abundance of massive galaxies in IllustrisTNG, aside from the slightly larger volume (1.4 times that of EAGLE).

Moving our focus to disc galaxies, we notice that EAGLE and IllustrisTNG discs systematically occupy the high end of the f_* distribution, having on average 35% (0.13 dex) higher f_* than the typical simulated galaxy with the same stellar mass.

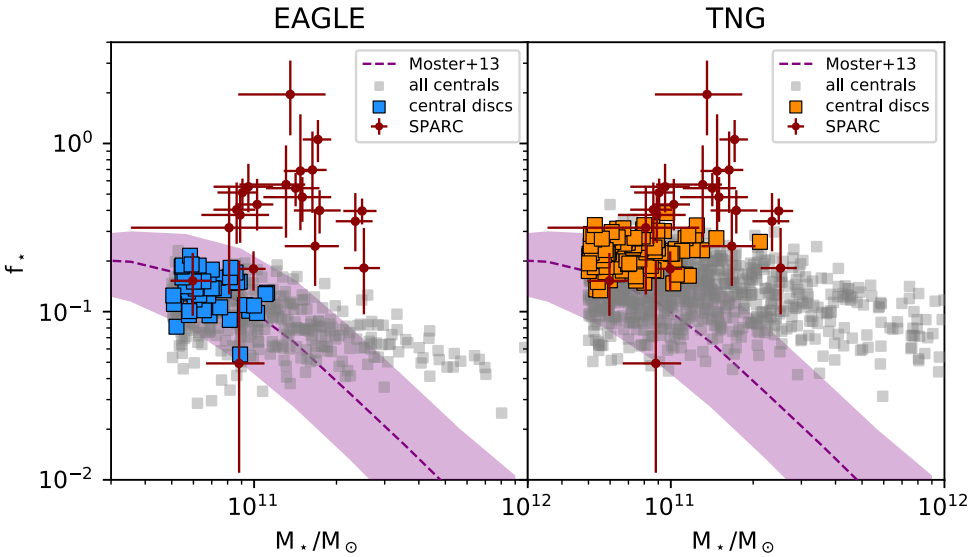


Fig. 2. Stellar fraction as a function of the stellar mass for simulated (central) galaxies in EAGLE (left panel) and IllustrisTNG (right panel) with $M_\star > 5 \times 10^{10} M_\odot$, compared to nearby spirals from the SPARC dataset (red circles with error-bar). Coloured symbols are used for our subsample of simulated discs. The purple shaded region shows the AM relation and related scatter from Moster et al. (2013).

However, this is not enough to match the exceptionally high f_\star of the observed spirals. The mismatch is expected given the offset in the TFR at high M_\star (Fig. 1), but is also due to an additional offset in the $v_{\text{flat}} - M_{\text{halo}}$ relation which implies that, at a given v_{flat} , simulated discs inhabit more massive halos than real ones. The combination of these two effects produces the mismatch observed.

Simulated discs partially overlap with the data in the (f_\star, M_\star) plane, but the comparison is limited as the former are very rare at $M_\star > 10^{11} M_\odot$ (see Section 4). Lowering the thresholds in \mathcal{R}_\star and \mathcal{F}_\star would allow for a larger sample of discs at higher M_\star , but these would not compare favourably with SPARC given that the observed and simulated populations diverge significantly at higher masses. At $1 < M_\star / M_\odot < 3 \times 10^{11}$, the median f_\star of EAGLE (IllustrisTNG) discs is 0.13 (0.23), while in SPARC it is 0.48, with some individual systems reaching unity. These considerations highlight the difficulty of producing massive disc galaxies in numerical simulations with the observed global stellar-to-dark matter mass ratio.

3.2. Local disc-halo connection

Additional insights into the disc-halo connection can be obtained by studying the mass distribution at local scales, i.e. within the galaxy discs. In Fig. 3 we show how the ratio between the stellar mass $M_\star(R)$ and the total dynamical mass $M_{\text{dyn}}(R)$ enclosed within a given radius R varies as a function of R for the massive discs in SPARC and in the simulations. For SPARC galaxies we derive $M_\star(R)$ from their $3.6 \mu\text{m}$ surface brightness profile assuming a razor-thin disc geometry and mass-to-light ratios from PFM19. Provided that the contribution of the gas to the mass budget within the disc is very small, we set $M_{\text{dyn}}(R) \approx M_\star(R) + R(v_{\text{obs}}^2 - v_\star^2)/G$. In the simulations, instead, we compute enclosed masses directly from the particle data.

Fig. 3 clearly shows that the simulations underestimate the contribution of stars to the total mass budget at all radii. The discrepancy is a factor of ~ 2 between 1 and $2 \times$ the effective radius (R_{eff}), and decreases down to a factor 1.5 at smaller and

larger radii. Simulated discs already become dark matter dominated at $R \sim 5 \text{ kpc}$, while stars in SPARC spirals constitute the main dynamical component out to $R \sim 15 \text{ kpc}$. This implies that not only simulated discs inhabit heavier halos than observed, but that also the internal dynamics of these discs on local scales is more dark matter-dominated than observed. In this context, the offset in the size- M_\star relation noticeable from Fig. 1 plays an important role since, at a given M_\star , larger discs have lower stellar surface densities corresponding to lower radial acceleration at any given radius. Furthermore, the concentrations inferred from a decomposition of the rotation curves of simulated galaxies (Appendix B) are a factor of ~ 2 higher than those determined for SPARC galaxies of the same inferred M_{halo} . This drives down $M_\star(R)/M_{\text{dyn}}(R)$ even further in the inner galactic regions.

This local discrepancy is another important manifestation of the peculiar galaxy-halo connection of massive discs, which is coupled to the global discrepancy already noted by PFM19. Our new findings on the local stellar-to-dynamical mass ratio are important in this context, since while one might argue that to solve the f_\star discrepancy on global scales discs would need to inhabit even higher-concentration halos (so that the same circular velocity is obtained in less massive halos), this would further exacerbate the $(M_\star/M_{\text{dyn}})($R)$ discrepancy on local scales, ruling this out as a viable solution. Thus, all of our results combined suggest that, in order to explain their observed properties, massive spirals need to have *everywhere* less dark matter than expected from AM models.$

4. Discussion and Summary

The relation between the stellar and the dark matter masses in nearby disc galaxies seem to be well described by a simple power law (Posti et al. 2019b), which translates into a monotonic relation between M_\star and the star formation efficiency f_\star (PFM19). As a consequence, massive ($M_\star \gtrsim 5 \times 10^{10} M_\odot$) spirals depart significantly from the predictions of AM methods, reaching f_\star of about unity at the high- M_\star end (failed feedback problem). This result is largely independent of the halo profile model adopted in the kinematic decomposition, as we did also

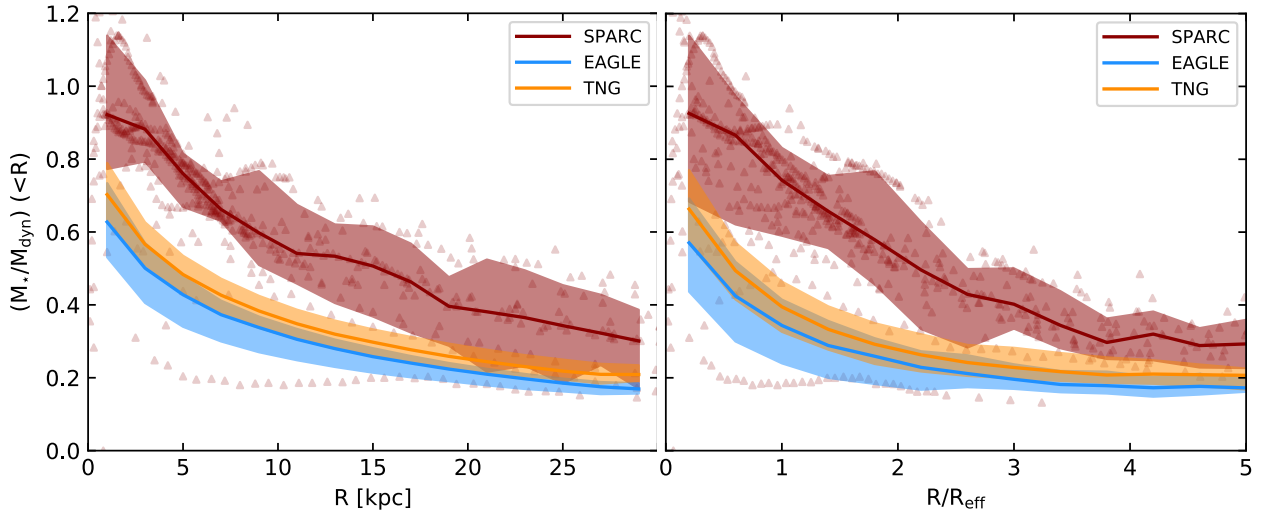


Fig. 3. *Left panel:* Stellar-to-total enclosed mass profiles for massive disc galaxies in the EAGLE (blue) and IllustrisTNG (orange) simulations, compared with the data from SPARC (red). The solid lines show the median profiles, while the shaded areas represent the scatter given by the difference between the 84th and the 16th percentiles. Individual measurements for SPARC spirals are shown as red triangles. *Right panel:* As in the left panel, but radii are normalised to the effective radius R_{eff} of each galaxy.

verify using the various mass models provided by [Ghari et al. \(2019\)](#) and [Li et al. \(2020\)](#) for the SPARC dataset.

In this work we have analyzed this discrepancy, both on a global and local scale, comparing observations with predictions from two of the best-known recent cosmological hydrodynamical simulations, EAGLE and IllustrisTNG, which each resolve the internal structure and dynamics of several tens of massive spirals. Our results show that simulated discs appear to inhabit overly massive dark matter halos, and that their dynamics, unlike real spirals, are everywhere dark matter dominated by a wide margin.

In the simulations we have computed stellar and halo masses using two different approaches: we have extracted them directly from the galaxy catalogues and have determined them via a mass-decomposition of circular velocity profiles. The two methods lead to compatible results (see Fig. B.1), which incidentally validates the approach adopted by [PFM19](#) for their analysis. However, rotation curves in SPARC are determined from $\text{H}\alpha$ (and, in part, $\text{H}\alpha$) data, and one may argue that tracing the azimuthal speed of cold gas in the simulated galaxies, rather than extracting their v_c profile, would lead to a more direct comparison with the observations. We have checked this using the approach described by [Oman et al. \(2019\)](#) to derive the $\text{H}\alpha$ content of the gas particles in the simulations, and measured the $\text{H}\alpha$ rotational speed in annuli of 1 kpc width oriented according to the $\text{H}\alpha$ angular momentum vector of each galaxy. Unfortunately, we found that the $\text{H}\alpha$ kinematics of simulated discs is strongly disturbed (especially in EAGLE) and only in rare cases approaches the circular velocity. The reasons for this remain to be clarified, but may well be related to disturbances induced by over-efficient feedback from the central black holes, which is in fact the main suspect for the f_\star mismatch between simulated and observed massive spirals.

Another explanation for the lack of massive discs with high f_\star in the models may be that the SPARC sample, which is not volume-limited, is made of rare, special systems that are not representative of the overall population of spirals. A simple argument demonstrates that this is not the case: 13 out of the 21 high- f_\star SPARC galaxies are located within a distance of 62 Mpc,

which encompasses a spherical volume equivalent to those of the runs studied here. The systematic lack of these objects in the simulations must therefore be due to a deficiency of the models, rather than to a bias in the observations.

We have shown that the discrepancy in the stellar-to-dark matter ratio between simulated and observed systems is both global and local, and extends well into their inner regions where the former are dark-matter dominated at all radii (except for the innermost ~ 5 kpc), while in the latter the stellar component dominates the galaxy dynamics. The dynamical importance of stars in observed massive spirals is well known and emerges directly from the shape of their rotation curves, which follows very closely the light profile (the so-called Renzo's rule, [Sancisi 2004](#)) for several kpc before flattening out. The small-scale discrepancy was already outlined by [Ludlow et al. \(2017\)](#) when investigating the radial acceleration relation ([McGaugh et al. 2016](#)) in EAGLE discs, by [Lovell et al. \(2018\)](#) for high-mass IllustrisTNG galaxies, and seems to be even stronger in other simulation suites such as SIMBA ([Davé et al. 2019; Glowacki et al. 2020](#)). Here, we have highlighted how the problem exists at all scales. Clearly, at a fixed f_\star , differences in the halo density profiles and in the disc sizes can lead to very diverse M_\star/M_{dyn} profiles, thus the relation between small and large scales is not trivially set by f_\star . The simulated halos appear to be highly concentrated, probably as a result of halo contraction, which represents a plausible explanation for the discrepancy with observations in the regions of the discs.

It is possible to draw a parallel between these simulated discs and another category of dark matter-dominated objects: dwarf galaxies. The dominance of dark matter in the simulated discs results in a poor variety in their circular velocity profiles (not shown in this work). As the star formation efficiency of the host halos is nearly constant (Fig. 2), this results in a very narrow TFR (Fig. 1) and little scatter in the M_\star/M_{dyn} profiles (Fig. 3). In contrast, the observed galaxies seem to show more variety in their f_\star , rotation curves and M_\star/M_{dyn} profiles. This echoes the ‘diversity problem’ for dwarf galaxies ([Oman et al. 2015](#)), where the self-similar shape of v_c profiles in simulated dwarfs is in tension with the diversity in the $\text{H}\alpha$ rotation curves that can

be found in the observed population, at a fixed rotational speed. There are however two important differences between the low- and high-mass regimes. The first is that the H I kinematics of in dwarf galaxies is typically more disturbed (Oh et al. 2015; Iorio et al. 2017), and this results in more uncertain rotation curves which can be, to some extent, model-dependent (e.g. Spekkens & Sellwood 2007). The second is that the diversity problem in dwarfs is closely related to the cusp-core issue (Flores & Primack 1994; Moore 1994), which concerns the innermost central regions of dwarfs, whereas the discrepancy at the high-mass end is both local and global.

The results of PFM19 suggest the existence of different pathways for the creation of massive late-type and early-type systems, with the former resulting from more gentle merging histories which would lead to lower dark matter content and higher star formation efficiencies. We note that such a scenario is not inconsistent with the existence of a unique SHMR (with scatter), as predicted by current Λ CDM models. As discussed by Moster et al. (2019), active and passive systems are expected to distribute differently within the scatter of the SHMR due to the diverse accretion histories of their halos. This effect, combined with the shallow slope of the SHMR at large masses, is such that at a fixed M_\star active (passive) galaxies at $z=0$ are scattered preferentially towards lower (higher) halo masses, in line with the observed trend. However, at a M_\star of $10^{11} M_\odot$, this should lead to a difference of ~ 0.2 dex in the f_\star of active and passive galaxies, which is approximately what we find comparing our EAGLE and IllustrisTNG discs with the whole population of centrals at similar M_\star , but is largely insufficient to justify the difference between the AM prediction and the observed data.

It is possible, though, that a larger scatter in the SHMR may help in reconciling observations and theory. Indeed, the recent discovery of super-spirals (Ogle et al. 2019b), which are extremely massive ($\log(M_\star/M_\odot) > 11.5$) late-type systems with rotational speed up to $\sim 570 \text{ km s}^{-1}$ (Ogle et al. 2019a), suggests that the population of high- M_\star disc galaxies is more heterogeneous than previously thought. Such systems must be rare, as only 3 objects with H I velocity width (W_{50}) larger than 800 km s^{-1} are present in the ALFALFA-100 catalogue (Haynes et al. 2018). Yet, their existence is symptomatic of a wider distribution of feedback efficiencies at fixed halo mass. In the specific case of the massive spirals considered here, less efficient feedback from stars and/or AGNs can help in bringing the models closer to the data on both global and local scales, leading to higher stellar masses at fixed halo mass and to smaller disc sizes due to less efficient angular momentum redistribution from the outer to the inner regions of the halo's gas reservoir (e.g. Brook et al. 2012). While a lower feedback efficiency may alleviate the problems discussed in this work, the way it would affect other galaxy properties remains to be clarified. For instance, different theoretical models of galaxy evolution give very different predictions for the growth of discs in the absence of galaxy-scale, powerful feedback episodes (e.g. Navarro & Steinmetz 1997; Pezzulli et al. 2017).

In summary, our findings indicate that the population of high-mass spirals emerging from state-of-the-art Λ CDM cosmological simulations differs systematically from that which we observe in terms of both local and global stellar-to-dark matter content. The difference cannot be explained in terms of selection effects or limitations in the modelling of the observed data, and clearly points to a mismatch in the efficiency of massive spirals at converting their baryons into stars. Ultimately, this difference can be understood in terms of a more scattered galaxy-halo connection at the high end of the stellar mass function, which, at the

current stage, does not seem to emerge from numerical models in Λ CDM framework.

Acknowledgements. AM and GC acknowledge the support by INAF/Frontiera through the "Progetti Premiali" funding scheme of the Italian Ministry of Education, University, and Research. BF acknowledges funding from the Agence Nationale de la Recherche (ANR project ANR-18-CE31-0006 and ANR-19-CE31-0017) and from the European Research Council (ERC) under the European Union's Horizon 2020 research and innovation programme (grant agreement No. 834148). LP acknowledges support from the Centre National d'Etudes Spatiales (CNES). KO acknowledges support by the European Research Council (ERC) through Advanced Investigator grant to C.S. Frenk, DMIDAS (GA 786910).

References

Bahé, Y. M., Crain, R. A., Kauffmann, G., et al. 2016, MNRAS, 456, 1115
 Behroozi, P. S., Conroy, C., & Wechsler, R. H. 2010, ApJ, 717, 379
 Brook, C. B., Stinson, G., Gibson, B. K., et al. 2012, MNRAS, 419, 771
 Cappellari, M., Scott, N., Alatalo, K., et al. 2013, MNRAS, 432, 1709
 Crain, R. A., Schaye, J., Bower, R. G., et al. 2015, MNRAS, 450, 1937
 Davé, R., Anglés-Alcázar, D., Narayanan, D., et al. 2019, MNRAS, 486, 2827
 Diemer, B., Stevens, A. R. H., Lagos, C. d. P., et al. 2019, MNRAS, 487, 1529
 Driver, S. P., Hill, D. T., Kelvin, L. S., et al. 2011, MNRAS, 413, 971
 Dutton, A. A., Conroy, C., van den Bosch, F. C., Prada, F., & More, S. 2010, MNRAS, 407, 2
 Dutton, A. A. & Macciò, A. V. 2014, MNRAS, 441, 3359
 Flores, R. A. & Primack, J. R. 1994, ApJ, 427, L1
 Ghari, A., Famaey, B., Laporte, C., & Haghī, H. 2019, A&A, 623, A123
 Glowacki, M., Elson, E., & Davé, R. 2020, The baryonic Tully-Fisher relation in the Simba simulation
 Haynes, M. P., Giovanelli, R., Kent, B. R., et al. 2018, ApJ, 861, 49
 Iorio, G., Fraternali, F., Nipoti, C., et al. 2017, MNRAS, 466, 4159
 Kravtsov, A. V., Vikhlinin, A. A., & Meshcheryakov, A. V. 2018, Astronomy Letters, 44, 8
 Leauthaud, A., Tinker, J., Bundy, K., et al. 2012, ApJ, 744, 159
 Lelli, F., McGaugh, S. S., & Schombert, J. M. 2016, AJ, 152, 157
 Li, P., Lelli, F., McGaugh, S., & Schombert, J. 2020, ApJS, 247, 31
 Lovell, M. R., Pillepich, A., Genel, S., et al. 2018, MNRAS, 481, 1950
 Ludlow, A. D., Benítez-Llambay, A., Schaller, M., et al. 2017, Phys. Rev. Lett., 118, 161103
 Mandelbaum, R., Seljak, U., Kauffmann, G., Hirata, C. M., & Brinkmann, J. 2006, MNRAS, 368, 715
 Mandelbaum, R., Wang, W., Wu, Y., et al. 2016, MNRAS, 457, 3200
 McAlpine, S., Helly, J. C., Schaller, M., et al. 2016, Astronomy and Computing, 15, 72
 McGaugh, S. S., Lelli, F., & Schombert, J. M. 2016, Phys. Rev. Lett., 117, 201101
 Moffett, A. J., Ingarfield, S. A., Driver, S. P., et al. 2016, MNRAS, 457, 1308
 Moore, B. 1994, Nature, 370, 629
 More, S., van den Bosch, F. C., Cacciato, M., et al. 2011, MNRAS, 410, 210
 Moster, B. P., Naab, T., & White, S. D. M. 2013, MNRAS, 428, 3121
 Moster, B. P., Naab, T., & White, S. D. M. 2019, arXiv e-prints, arXiv:1910.09552
 Navarro, J. F., Frenk, C. S., & White, S. D. M. 1996, ApJ, 462, 563
 Navarro, J. F. & Steinmetz, M. 1997, ApJ, 478, 13
 Nelson, D., Springel, V., Pillepich, A., et al. 2019, Computational Astrophysics and Cosmology, 6, 2
 Ogle, P. M., Jarrett, T., Lanz, L., et al. 2019a, ApJ, 884, L11
 Ogle, P. M., Lanz, L., Appleton, P. N., Helou, G., & Mazzarella, J. 2019b, ApJS, 243, 14
 Oh, S.-H., Hunter, D. A., Brinks, E., et al. 2015, AJ, 149, 180
 Oman, K. A., Marasco, A., Navarro, J. F., et al. 2019, MNRAS, 482, 821
 Oman, K. A., Navarro, J. F., Fattahi, A., et al. 2015, MNRAS, 452, 3650
 Persic, M., Salucci, P., & Stel, F. 1996, MNRAS, 281, 27
 Pezzulli, G., Fraternali, F., & Binney, J. 2017, MNRAS, 467, 311
 Pillepich, A., Springel, V., Nelson, D., et al. 2018, MNRAS, 473, 4077
 Planck Collaboration, Aghanim, N., Akrami, Y., et al. 2018, arXiv e-prints, arXiv:1807.06209
 Posti, L., Fraternali, F., & Marasco, A. 2019a, A&A, 626, A56
 Posti, L., Marasco, A., Fraternali, F., & Famaey, B. 2019b, A&A, 629, A59
 Read, J. I., Iorio, G., Agertz, O., & Fraternali, F. 2017, MNRAS, 467, 2019
 Sancisi, R. 2004, in IAU Symposium, Vol. 220, Dark Matter in Galaxies, ed. S. Ryder, D. Pisano, M. Walker, & K. Freeman, 233
 Schaye, J., Crain, R. A., Bower, R. G., et al. 2015, MNRAS, 446, 521
 Spekkens, K., & Sellwood, J. A. 2007, ApJ, 664, 204
 Springel, V. 2005, MNRAS, 364, 1105
 Springel, V. 2010, MNRAS, 401, 791
 Thob, A. C. R., Crain, R. A., McCarthy, I. G., et al. 2019, MNRAS, 485, 972
 Tully, R. B. & Fisher, J. R. 1977, A&A, 500, 105
 Vale, A. & Ostriker, J. P. 2004, MNRAS, 353, 189
 van den Bosch, F. C., Lange, J. U., & Zentner, A. R. 2019, MNRAS, 488, 4984
 van den Bosch, F. C., Norberg, P., Mo, H. J., & Yang, X. 2004, MNRAS, 352, 1302
 Wechsler, R. H. & Tinker, J. L. 2018, ARA&A, 56, 435
 White, S. D. M. & Rees, M. J. 1978, MNRAS, 183, 341

Appendix A: Supplementary material

Tables A.1 and A.2 list the main properties of the samples of simulated and observed massive disc galaxies studied in this work. These tables are available their entirety in machine-readable form at <https://drive.google.com/file/d/1qksA7yKmzQHRJQ3U3gXexW0e0hW9RnVs/view?usp=sharing>.

In Fig. A.1 and A.2 we show face- and edge-on images for four representative massive disc galaxies extracted from the simulated sample studied in this work, along with their circular velocity profiles, truncated at the expected H_I radius, decomposed into the contributions from stars, gas and dark matter. A full database of such figures for all simulated galaxies studied here can be freely downloaded at <https://drive.google.com/file/d/1WvnwRwAnOpEcGU9OTI-GHKf0w7-Ihlxn/view?usp=sharing>.

Appendix B: Mass decomposition of synthetic rotation curves

We show here that our results do not change if we compute stellar and halo masses in the simulations using a procedure analogous to that of PFM19, based on the mass-decomposition of rotation curves. To do so, we consider the synthetic rotation curves of our simulated galaxies truncated at their expected HI radius (see Section 2) and model them as

$$v_c = \sqrt{v_{\text{DM}}^2 + v_{\star}^2 + v_{\text{gas}}^2} \quad (\text{B.1})$$

where v_{DM} , v_{\star} and v_{gas} are, respectively, the contributions of dark matter, stars and gas to the circular velocity profile.

As in PFM19, we assume Navarro-Frank-White (NFW, Navarro et al. 1996) dark matter halo profiles. These are fully described by their virial mass M_{200} and their concentration c , both of which are free parameters of the model. We assume $v_{\star} = \sqrt{\Upsilon v_{\star,\text{true}}^2}$, where $v_{\star,\text{true}}^2$ is given by $GM_{\star}(< R)/R$ and is assumed to be known, and Υ is a free parameter that mimics the effect of a (radially-constant) mass-to-light ratio. With this parametrization, deviations from $\Upsilon = 1$ correspond to variations in the inferred stellar mass with respect to its true value. Finally, we fix v_{gas}^2 to its true value ($GM_{\text{gas}}(< R)/R$) as this gives only a minor contribution to the v_c . Following PFM19, the three free parameters of the model (M_{200} , c and Υ) are fit to the data via a Bayesian approach which adopts a prior on the $c - M_{200}$ relation motivated by N-body cosmological simulations (Dutton & Macciò 2014).

In the top panels of Fig. B.1 we compare the stellar and halo masses derived with this method with their ‘true’ values taken from the simulation catalogues. Clearly, there is excellent agreement between true and inferred masses with consequently little variation in the $f_{\star} - M_{\star}$ relation (bottom panels of Fig. B.1). We notice systematic shifts upwards for the inferred values of f_{\star} , with typical $\delta f_{\star}/f_{\star}$ of 0.22 in EAGLE and 0.29 in IllustrisTNG, which however fall well within the quoted uncertainties. This is a confirmation of the validity of the PFM19 method, and indicates that NFW halos, in the mass range considered here, are good proxies for the dark matter density profiles in EAGLE and IllustrisTNG.

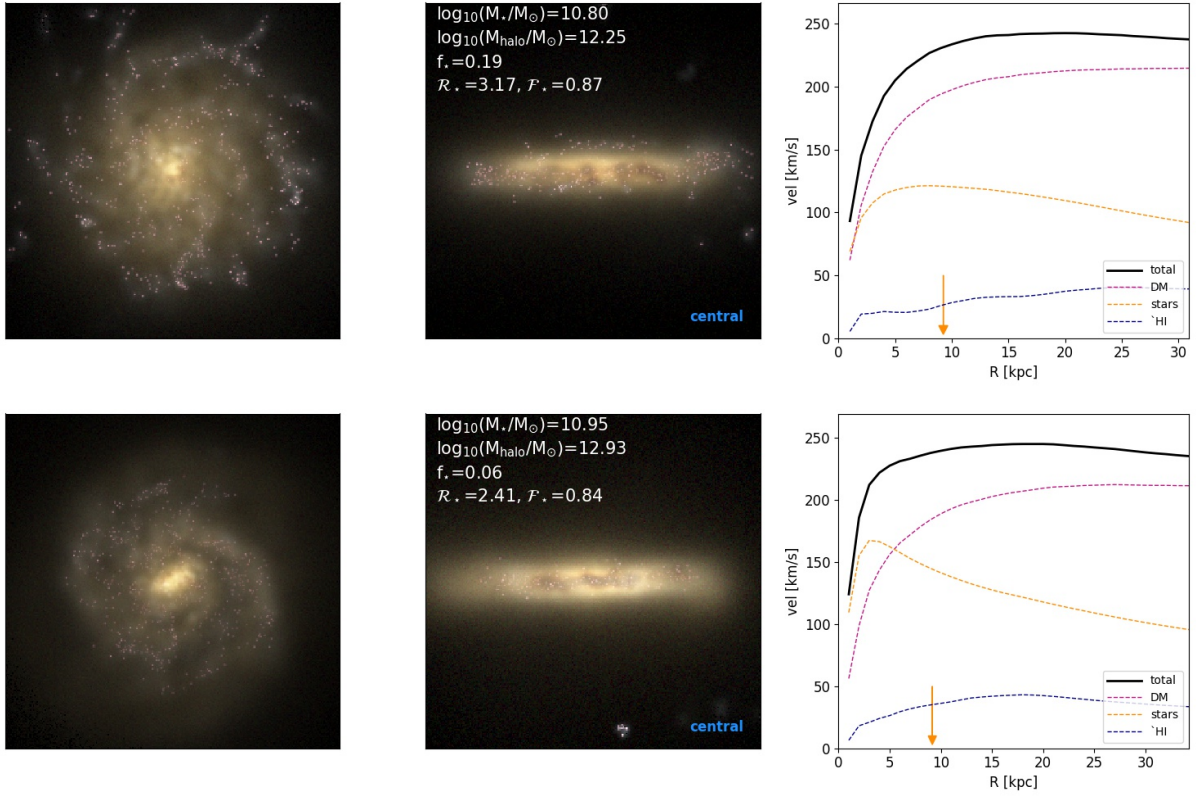


Fig. A.1. Two examples of massive (central) disc galaxies from the EAGLE simulations (run Ref-L0100N1504). The left and central panels show the systems from a face- and edge-on perspective. The right panels show the total circular velocity profiles (solid black lines), along with the separate contributions (dashed lines) from stars (orange), gas (blue) and dark matter (magenta). The vertical arrow shows the half- M_\star radius.

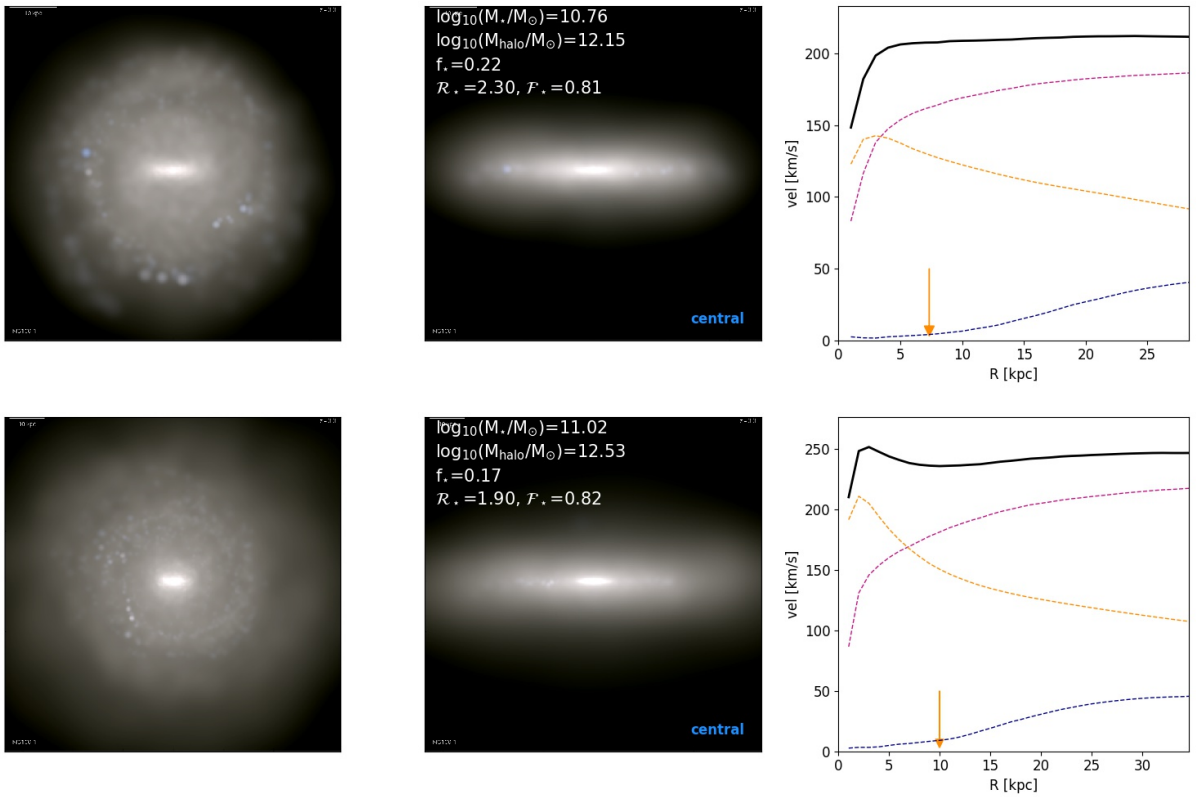


Fig. A.2. As in Fig. A.1, but for two massive (central) discs from the IllustrisTNG simulations (run TNG100-1).

Table A.1. Main properties of the sample of simulated massive discs studied in this work.

Simulation (1)	Galaxy ID (2)	$\log_{10}(M_\star/M_\odot)$ (3)	$\log_{10}(M_{\text{halo}}/M_\odot)$ (4)	v_{flat} (5)	R_{eff} (6)	\mathcal{R}_\star (7)	\mathcal{F}_\star (8)
EAGLE	14582105	10.95	12.93	236.66	9.17	2.41	0.84
EAGLE	14202038	10.98	12.70	253.67	9.24	2.50	0.83
EAGLE	15518507	11.01	12.74	287.68	13.45	2.32	0.79
		...					
IllustrisTNG	351452	11.11	12.48	266.92	9.20	1.75	0.82
IllustrisTNG	368436	11.33	12.64	290.15	16.58	1.79	0.84
IllustrisTNG	369366	10.89	12.25	225.96	13.18	1.82	0.89
		...					

Notes. (1) Simulation suite, the runs analysed are Ref-L0100N1504 in EAGLE and TNG100-1 in IllustrisTNG; (2) galaxy ID from the catalogues of [McAlpine et al. \(2016\)](#) and [Nelson et al. \(2019\)](#); (3)-(4) stellar and halo masses; (5) Velocity of the flat part of the rotation curve in km s^{-1} , defined as specified in Section 2; (6) effective (half-mass) stellar radius in kpc; (7)-(8) mean stellar v/σ and stellar disc fraction, defined as in Section 2.

Table A.2. Main properties for the sample of massive nearby spirals studied in this work.

Galaxy (1)	$\log_{10}(M_\star/M_\odot)$ (2)	$\epsilon_{M_\star, \text{low}}$ (3)	$\epsilon_{M_\star, \text{up}}$ (4)	$\log_{10}(M_{\text{halo}}/M_\odot)$ (5)	$\epsilon_{M_{\text{halo}}, \text{low}}$ (6)	$\epsilon_{M_{\text{halo}}, \text{up}}$ (7)	v_{flat} (8)	$\epsilon_{v_{\text{flat}}}$ (9)	R_{eff} (10)	$\epsilon_{R_{\text{eff}}}$ (11)
NGC 7331	10.78	10.69	10.84	12.38	12.21	12.60	239.00	5.40	3.99	0.41
NGC 5985	10.91	10.55	11.10	12.21	12.12	12.28	293.60	8.60	10.71	2.67
UGC 03205	10.94	10.85	11.00	12.12	11.95	12.33	219.60	8.60	5.35	1.07
UGC 11914	10.95	10.82	11.04	13.04	12.44	13.67	288.10	10.50	3.12	0.94
UGC 05253	10.95	10.81	11.05	12.16	12.08	12.27	213.70	7.10	4.28	1.07
NGC 5907	10.96	10.87	11.01	12.02	11.93	12.16	215.00	2.90	7.88	0.41
NGC 2998	10.98	10.85	11.07	12.01	11.91	12.13	209.90	8.10	7.06	1.06
NGC 2841	11.00	10.95	11.04	12.54	12.42	12.69	284.80	8.60	5.51	0.55
NGC 3992	11.01	10.93	11.07	12.15	12.03	12.30	241.00	5.20	9.99	0.97
UGC 12506	11.12	10.95	11.19	12.14	11.96	12.33	234.00	16.80	12.36	1.24
NGC 5371	11.13	10.94	11.26	11.64	11.53	11.74	209.50	3.90	9.80	2.45
UGC 09133	11.15	11.04	11.24	12.22	12.18	12.25	226.80	4.20	5.92	1.18
NGC 2955	11.17	11.11	11.22	12.13	11.80	12.48	— ^a	— ^a	7.22	0.72
UGC 02953	11.18	11.03	11.28	12.29	12.22	12.36	264.90	6.00	5.03	1.51
NGC 6195	11.21	11.15	11.26	12.16	11.94	12.42	251.70	9.30	9.52	0.95
UGC 11455	11.22	11.11	11.31	12.61	12.43	12.84	269.40	7.40	10.06	1.51
NGC 0801	11.23	11.18	11.28	12.00	11.90	12.14	220.10	6.20	7.76	0.78
NGC 6674	11.24	11.15	11.32	12.42	12.32	12.56	241.30	4.90	7.75	1.54
UGC 02885	11.37	11.30	11.43	12.62	12.48	12.79	289.50	12.00	12.20	1.22
UGC 02487	11.39	11.33	11.45	12.58	12.52	12.67	332.00	3.50	9.63	1.45
ESO 563-G021	11.40	11.33	11.46	12.93	12.70	13.21	314.60	11.70	10.59	1.59

Notes. (1) Galaxy name; (2)-(4) stellar mass and related lower and upper uncertainties from [PFM19](#); (5)-(7) halo mass and related lower and upper uncertainties from [PFM19](#); (8)-(9) velocity of the flat part of the rotation curve (in km s^{-1}) and related uncertainty from [Lelli et al. \(2016\)](#); (6) effective radius (in kpc) and related uncertainty from [Lelli et al. \(2016\)](#).

^a The rotation curve of NGC 2955 does not have a well defined flat part, thus its v_{flat} is not reported in [Lelli et al. \(2016\)](#).

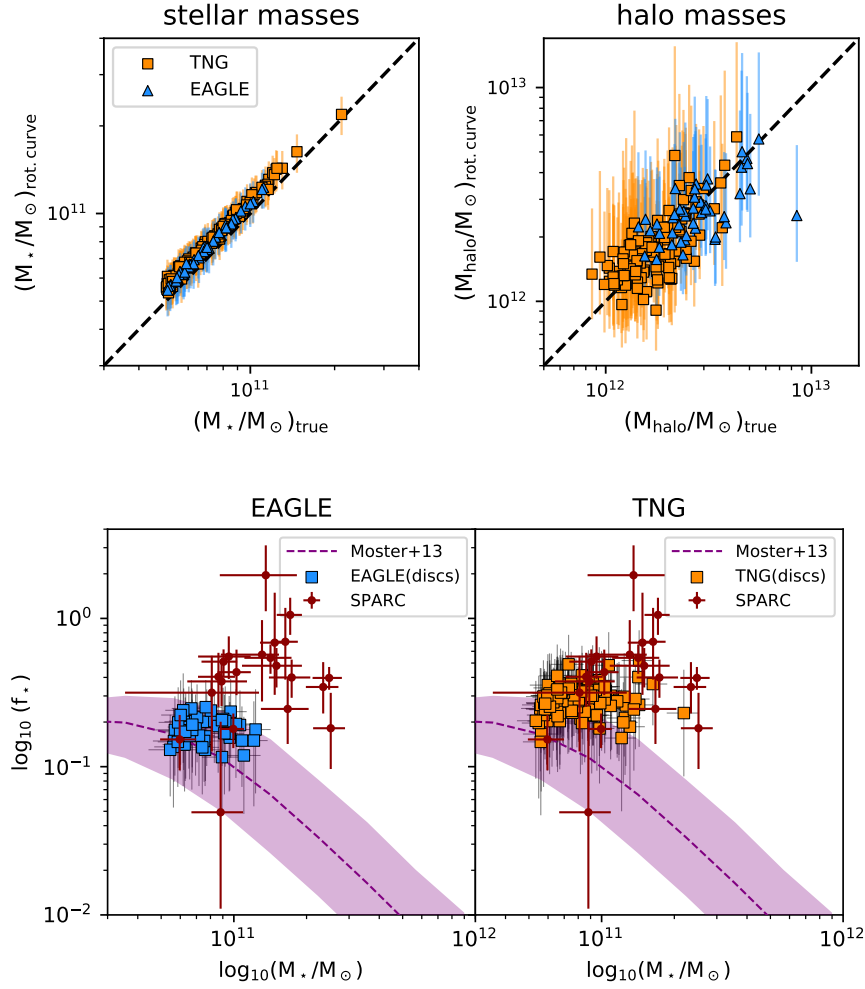


Fig. B.1. Top-left panel: comparison between the ‘true’ stellar masses of the simulated disc galaxies (x-axis) and those derived via the decomposition of their synthetic rotation curve (y-axis). EAGLE (IllustrisTNG) galaxies are shown as blue triangles (orange squares). Error-bars are given from the difference between the 84th and 16th percentiles in the posterior probability distributions. The dashed line shows the one-to-one relation. Top-right panel: the same, but for the halo masses. Bottom panels: f_* – M_* plot for the simulated discs using stellar and halo masses from rotation curve decomposition. Colors and symbols are as in Fig. 2.